REPORT DOCUMENTATION PAGE

Form Approved
OMB No. 0704-0188

1. REPORT DATE *(DD-MM-YYYY)*
29-04-2004

REPRINT

4. TITLE AND SUBTITLE
ESTIMATING VELOCITY TURBULENCE MAGNITUDES USING THE THERMOSONDE

5a. CONTRACT NUMBER

5b. GRANT NUMBER

5c. PROGRAM ELEMENT NUMBER
62601F

6. AUTHOR(S)
G. Jumper, J. Roadcap, P. Tracy and J. P. McHugh*

5d. PROJECT NUMBER
1010

5e. TASK NUMBER
0T

5f. WORK UNIT NUMBER
A1

7. PERFORMING ORGANIZATION NAME(S) AND ADDRESS(ES)
Air Force Research Laboratory/VSBY
29 Randolph Road
Hanscom AFB MA 01731-3010

8. PERFORMING ORGANIZATION REPORT

20040518 086

9. SPONSORING / MONITORING AGENCY NAME(S) AND ADDRESS(ES)

10. SPONSOR/MONITOR'S ACRONYM(S)
AFRL/VSBY

11. SPONSOR/MONITOR'S REPORT NUMBER(S)
AFRL-VS-HA-TR-2004-1054

12. DISTRIBUTION / AVAILABILITY STATEMENT
Approved for Public Release; Distribution Unlimited.

*Mechanical Engineering Department, Univ of New Hampshire, Durham, NH

13. SUPPLEMENTARY NOTES
REPRINTED FROM: PROCEEDINGS 41ST AEROSPACE SCIENCES MEETING AND EXHIBIT, 6-9 January 2003, Reno, NV (AIAA 2003-0191).

14. ABSTRACT
Equations are developed to estimate velocity turbulence from index of refraction turbulence as measured by the thermosonde. Using an adaptation of the radar ''power'' method to estimate velocity fluctuations from backscattered radar return and concurrently measured atmospheric data, the method is applied to optical turbulence measured by the thermosonde. The method is then used to compare velocity turbulence levels as estimated by the thermosonde to those estimated by the ''GroundWinds'' lidar in the lee of Mt. Washington in New Hampshire. There is reasonable agreement in identification of the areas of high turbulence.

15. SUBJECT TERMS
Optical turbulence Thermosonde LIDAR

16. SECURITY CLASSIFICATION OF:			**17. LIMITATION OF ABSTRACT**	**18. NUMBER OF PAGES**	**19a. NAME OF RESPONSIBLE PERSON**
a. REPORT UNCLAS	UNCLAS	**c. THIS PAGE** UNCLAS	SAR	10	George Jumper
					19b. TELEPHONE NUMBER *(include area code)* 781-377-3148

AFRL-VS-HA-TR-2004-1054

AIAA 2003-0191
Estimating Velocity Turbulence Magnitudes Using the Thermosonde

G. Jumper, J. Roadcap, and P. Tracy
Air Force Research Laboratory
Battlespace Environment Division
Hanscom AFB, MA

John P. McHugh
Mechanical Engineering Department
University of New Hampshire

41st Aerospace Sciences Meeting & Exhibit
6 – 9 January 2003

Estimating Velocity Turbulence Magnitudes Using the Thermosonde

George Y. Jumper[*], John R. Roadcap[*], and Paul Tracy[‡]
Air Force Research Laboratory
Hanscom AFB, MA 01731-3010

And

John P. McHugh[#]
Mechanical Engineering Department
University of New Hampshire

ABSTRACT

Equations are developed to estimate velocity turbulence from index of refraction turbulence as measured by the thermosonde. Using an adaptation of the radar "power" method to estimate velocity fluctuations from backscattered radar return and concurrently measured atmospheric data, the method is applied to optical turbulence measured by the thermosonde. The method is then used to compare velocity turbulence levels as estimated by the thermosonde to those estimated by the "GroundWinds" lidar in the lee of Mt. Washington in New Hampshire. There is reasonable agreement in identification of the areas of higher turbulence.

NOMENCLATURE

A	=	Constant or coefficient
a	=	Constant or coefficient
C_x^2	=	Structure constant of the quantity x [units of $x^2/m^{2/3}$]
$D_x(r)$	=	Structure function of quantity x [units of x squared]
d	=	Distance [m]
g	=	Acceleration of gravity [m/s^2]
K	=	Ratio of specific heats C_p/C_v [n.d.]
k	=	Spatial wave number [m^{-1}]
M	=	Gradient of refractive index [m^{-1}]
N	=	Brunt-Väisälä Frequency [s^{-1}]
n	=	Index of refraction [n. d.]
P	=	Pressure or partial pressure when subscripted [Pa]
q	=	Specific humidity [n.d.]
$S_x(k)$	=	One-sided, one-dimensional spatial power spectrum of x
T	=	Temperature [K]
U, V	=	Components of mean horizontal wind velocity [m/s]
u	=	Fluctuating part of horizontal wind [m/s]
x	=	Distance (m)
Z	=	Altitude in Plots (km)
z	=	Distance in vertical direction (m)
ε	=	Turbulent kinetic energy dissipation rate [W kg^{-1} or m^2s^{-3}]
γ	=	Constant in $C_n^2 - \varepsilon$ relationship [n.d.]
λ	=	Wavelength of refracted radiation [m]
θ	=	Potential temperature [K]

Subscripts:

d	=	Dry air
n	=	Index of refraction
T	=	Temperature
U or u	=	Velocity
wv	=	Water vapor

Superscripts:

Bar	=	Time averaged or mean component

INTRODUCTION

Turbulence in the atmosphere is difficult to forecast and difficult to measure. Atmospheric turbulence is the random fluctuation of the air mass caused by shear instabilities in jet streams or over mountains, by convective instabilities associated with thunderstorms, and by the breaking of buoyancy or "gravity" waves, especially at higher altitudes. The spatial structure of atmospheric turbulence is often characterized by the rate of turbulent kinetic energy dissipation per unit mass, often called the eddy dissipation rate, ε. While it refers to the conversion of turbulent kinetic energy to heat at the molecular level, it is implicitly tied to the magnitude of fluctuations throughout the range of turbulent scale sizes through turbulence theory.

---

[*] Program Manager, Battlespace Environment Division, Assoc. Fellow AIAA
[*] Technical Advisor, Battlespace Environment Division
[‡] Sr. Electronic Engineer, Battlespace Environment Division
[#] Professor, University of New Hampshire

Clear Air Turbulence (CAT), the effect of strong waves and turbulence in the atmosphere on air vehicles, is one particularly dangerous manifestation of turbulence. Forecast of CAT is the subject of continuing research by NOAA, NCAR and the U.S. Air Force and Navy. Many detection algorithms have been evaluated, and generally each algorithm exhibits a wide variation in performance. This is not only due to the complexity of the forecast problem, but also the means available to validate the performance, primarily pilot reports (PIREPs). These PIREPs depend on an aircraft being at the right place at the right time. The perceived severity of a CAT event is very dependent on the specific aerodynamic characteristics of the aircraft and the subjective judgment of the pilot. Also the events that usually get reported are at the more severe end of the possible spectrum of turbulence.

TURBULENT KINETIC ENERGY

At equilibrium, Kolmogorov hypothesized that turbulent kinetic energy cascades from the largest eddies, called the outer scale of the turbulence, to the smallest eddies, the inner scale, primarily by inertial processes[1]. At the inner scale, kinetic energy is converted to thermal energy by viscous dissipation at the dissipation rate, ε. By virtue of the Kolmogorov hypothesis, small-scale isotropy is also implied. When the velocity spectrum is within the inertial range (between the outer and inner scale), Kolmogorov reasoned by dimensional arguments that the one way, one dimensional power spectral density of longitudinal velocity fluctuations has the following functional relationship[2]:

$$S_u(k) = A\,\varepsilon^{2/3}\,k^{-5/3} \qquad (1)$$

where A is a constant equal to approximately ½. In the inertial range, the second order cross-stream and vertical components of velocity structure functions in the longitudinal direction are larger[3] by a factor of 4/3. In the large Reynolds numbers associated with the atmosphere, there can be a wide inertial range over which Equation 1 applies. Turbulent equilibrium implies that a constant level of turbulent kinetic energy has been reached and stays steady, ε is a constant, and the power spectral density stays constant within the inertial range and appears as a straight line of slope -5/3 on a log-log plot. The variance of the turbulent energy fluctuations in longitudinal velocity within the inertial range is determined by the equation:

$$\overline{u^2} = \int_0^\infty S_u(k)\,dk \qquad (2)$$

The spectra can also be expressed in terms of the velocity structure constant, C_u^2:

$$S_u(k) = 0.25\,C_u^2\,k^{-5/3} \qquad (3)$$

By comparison of Equations 1 and 3, $C_u^2 = a\varepsilon^{2/3}$, where a is four time A, or approximately 2.

The radar provides a means of remotely estimating turbulence on a continuous basis. There are two basic methods of estimating the velocity turbulence using radars[4], one from reflected power and the other using the spectral spread of the returned beam. The methodology of the first technique has been adapted to the thermosonde. In this paper we briefly introduce the radar backscatter or power method of obtaining turbulence strength, then describe the thermosonde instrument and the adaptation of the power method to the thermosonde. Finally estimates of the velocity turbulence are presented from a campaign in Bartlett, New Hampshire and compared to turbulence levels estimated using the Ground Winds Lidar in Bartlett.

THE RADAR POWER METHOD

The index of refraction, n, in the atmosphere can be written as[5]:

$$n = 1 + a_d(\lambda)P_d/T + a_{wv}(\lambda)P_{wv}/T \qquad (4)$$

where P is the partial pressure of either the dry air (d) or the water vapor (wv) and the a coefficients are the wavelength dependent coefficients for either the dry air or the water vapor. Fluctuations in the index of refraction are caused by fluctuations of either the density of the dry air, the concentration of water vapor in the air, or both. Radars detect fluctuations in the index of refraction of the view volume by Bragg scatter[6]. For VHF radars the backscatter will generally fall within the inertial sub range of the turbulence.

The basis of the reflected power method is that the fraction of transmitted power that is reflected back to the radar is proportional to the mean refractive index structure constant, C_n^2. Therefore, the method can only be used for calibrated radars. The measured C_n^2 is the mean value over the sampled volume of the atmosphere, which is determined by the beam spread and the range gates of the radar. Estimates of the maximum C_n^2 within the volume is then based on an estimate of the fraction of the volume that is actually turbulent. The actual form of the radar C_n^2 equation depends on the radar configuration[4].

The relationship of C_n^2 to ε invokes equilibrium and the relationships for the dissipation of turbulent kinetic energy and refractive index turbulence[3, 7]. Hocking and Mu[8] consolidated the relevant considerations into the formula:

$$C_n^2 = \frac{1}{\gamma}\frac{M^2}{N^2}\varepsilon^{2/3} \tag{5}$$

where N is the Brunt Väisälä frequency and M (at radar wavelengths) is the refraction index gradient, which are defined by the following equations:

$$N^2 = \frac{g}{\bar{\theta}}\frac{d\bar{\theta}}{dz} \tag{6}$$

$$M = -77.6\times10^{-8}\frac{P}{T}\left(\frac{\partial \ln\theta}{\partial z}\right)\left[1+\frac{15500q}{T}\left(1-\frac{1}{2}\frac{\partial \ln q/\partial z}{\partial \ln\theta/\partial z}\right)\right] \tag{7}$$

where θ is the potential temperature defined by the equation[9]:

$$\theta(Z) = T(Z)\left(\frac{P_s}{P(Z)}\right)^{(K-1)/K} \tag{8}$$

P_s is the reference pressure, usually 1000 hPa. Finally, γ in Equation 5 was assumed constant in the early literature, but is often expressed as a function of gradient Richardson Number[9], defined by:

$$Ri(z) \equiv \frac{N^2}{\left(dU/dz\right)^2 + \left(dV/dz\right)^2} \tag{9}$$

where U and V are mean horizontal wind components. Some of uncertainties of the radar power method arise from the uncertainties in the calibration of the microwave source, the estimate of the fraction of the atmosphere that is turbulent, the form of the γ parameter, and the requirement to rely on available balloon soundings to determine the temperature and humidity profiles, the gradient Richardson Number and the Brunt-Väisälä frequency[10]. Using balloon-borne *in situ* temperature and velocity turbulence measurements, Bertin, et al[11] deduce that the beam spread method, while suffering from some uncertainties, is probably more accurate than the power method that is used here. There is an extensive database of temperature variance measurements using the thermosonde. These data have also been used to estimate the velocity turbulence[8, 12].

THERMOSONDE MEASUREMENTS:

The thermosonde is designed to measure optical turbulence in the atmosphere, that is refraction turbulence in the visible or near visible wavelengths. For these wavelengths, the magnitude of the water vapor term in Equation 4 is so small that it hardly contributes to the index of refraction, except, perhaps, at very low altitudes over a body of water. While both pressure and temperature appear in Equation 4, fluctuations in pressure in the free atmosphere are small and they dissipate rapidly through acoustic processes. Therefore, *in situ* measurement of optical turbulence is, in practice, reduced to measurement of fluctuations in temperature.

Before covering the calculation of ε, we give a brief description of the thermosonde as implemented at the Air Force Research Laboratory[13,14]. Two wire probes, spaced one meter apart on a horizontal boom, sense temperature differences as the instrument ascends through the atmosphere at around 5m/s, towed by a balloon on a 110m line. The probes use 3.45μm diameter wire, which has a time constant of less than 1ms, at nominal ascent speeds and sea level conditions. The temperature difference is continuously averaged by an onboard analog RMS integrated circuit. The output of the RMS chip is transmitted back to the ground station at 1.2s intervals. Since the balloon-borne payload is attached to a meteorological radiosonde, concurrent wind velocity, pressure, mean temperature, and humidity information are also relayed to the ground station. The output of the RMS chip, when converted to the RMS temperature difference, is a running structure function. Assuming that the turbulence follows the Kolmogorov hypothesis, the structure function has the following form[15]:

$$D_T(d) = C_T^2\, d^{2/3} \tag{10}$$

where d is the distance between the points of measurement and $D_T(d)$ is the structure function and C_T^2 is the temperature structure constant. Since the thermosonde acquires temperature differences at a 1m separation, the magnitude of the 1m-structure function, $D_T(1\text{m})$, is the magnitude of the structure constant. The amplitude of balloon acquired temperature structure constant (C_T^2) typically varies from the thermosonde noise floor ($1\text{x}10^{-6}$ to $1\text{x}10^{-5}\text{K}^2/\text{m}^{2/3}$) to a maximum of around $0.01\text{K}^2/\text{m}^{2/3}$. Values below $1\text{x}10^{-5}\text{K}^2/\text{m}^{2/3}$ do not significantly affect optical propagation. Conversion of the temperature structure constant to the refractive index structure constant, C_n^2, depends on local pressure and temperature and the wavelength of the radiation that is being propagated. For radiation near the visible spectrum, when the contribution can safely be ignored

except, perhaps right over a body of water, it is customary to use the formula[12*]:

$$C_n^2 = \left(a_d(\lambda) P / T^2\right)^2 C_T^2 \qquad (11)$$

where $a_d(\lambda)$=79x10^{-8}K/Pa for visible and near IR wavelengths.

The computation of ε from the thermosonde eliminates some of the shortcomings of the comparable radar calculation. First, the response of the instrument is fast enough to eliminate the need to estimate the turbulent fraction of the atmosphere (it is unity). Second, the atmospheric sounding data are taken concurrently with the C_T^2 data. In addition, the calculation for the thermosonde does not require terms that include the contribution of water vapor to the index of refraction for radar wavelengths. Rather than computing ε directly from the temperature structure constant (as shown in Ref.12) we will simply extend the radar power method (as described in Ref.8). From Equation 5:

$$\varepsilon = \left[\gamma C_n^2 N^2 M^{-2}\right]^{3/2} \qquad (12)$$

For near visible wavelengths, humidity can be ignored, and M simplifies to:

$$M = -a_d(\lambda) \frac{P}{T\theta} \frac{\partial \theta}{\partial z} \qquad (13)$$

At this point, a discussion of the constant, γ, is in order. Ottersten[3] suggested the following form for γ:

$$\gamma = \frac{1}{a^2 \,\mathrm{Pr}} \left(\frac{\mathrm{Pr} - Ri}{Ri} \right) \qquad (14)$$

Experimental data suggest that for Ri<<1, the turbulent Prandtl number, Pr, is near unity. We follow Hocking and Mu[8] in keeping Pr =1 and use their expression for γ:

$$\gamma = \frac{1}{a^2} \left(\frac{1 - Ri}{Ri} \right) \qquad (15)$$

We also use H&M's value for the constant $a^2 = 7.33$. When they used this equation to analyze thermosonde data, they used Equation 15 for values of *Ri* less than 1. They maintained γ at zero for higher values of *Ri*. This, they argued, was to suppress regions of decaying turbulence, which should be the case for the higher values of *Ri*. We have sided with other authors[3,7,10] who have argued that gamma approaches a non-zero constant at the higher values of Ri, and we have maintained a value of γ equal to 1 above $Ri = 0.12$.

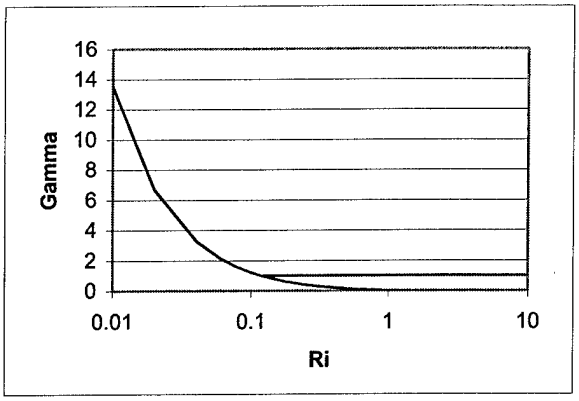

Figure 1: Plot of the Gamma factor versus the gradient Richardson number. As Ri decreases, the increasing values from Equation 15 are used. Above 0.12, γ is set to one.

As a final observation, when the equations for C_n^2, N^2, and M are substituted into Equation 12, we obtain the working equation:

$$\varepsilon = \left[\frac{\gamma C_T^2 \, g \, \theta}{\frac{d\theta}{dz} T^2} \right]^{3/2} \qquad (16)$$

Ultimately, the vertical variability in the estimated ε is due to the variability in both C_T^2 and the derivative of θ, with the former varying at the highest frequency.

THE EXPERIMENT

On 31 May 2001 thermosonde instruments were flown adjacent to the GroundWinds Lidar facility at the Bartlett, NH. This site is 24km south and slightly east of the summit of Mt. Washington, which is 1,917m above mean sea level (MSL). The GroundWinds site is 166m MSL. The experiment began at dusk, ~9pm EDT, with two thermosondes launched within 1 minute of each other. The next two thermosondes were launched right after 11pm. The best combination of lidar and thermosonde data was the 4th launch of the evening. A composite plot of mean air temperature and relative humidity, optical turbulence (C_n^2), wind speed and direction for the flight is shown in Figure 2. The results are quite distinct from "typical" thermosonde results, but they may be representative for flow in the lee of a good size mountain. In particular, up to about 4km, the optical turbulence levels are well above the

* In Reference 12, one of the square symbols (^{2}) was inadvertently omitted. Please correct it!

Clear1 model, the smooth curve in the C_n^2 plot. At 4km, twice the height of the mountain, the level drops dramatically to well below Clear1 until about 10km, perhaps 2km below the altitude of minimum temperature, which is the start of the tropopause region.

The lower 4km is quite active, and a good location to expect higher turbulence levels. An expanded view of the lowest 5km of the composite plot is shown in Figure 3. The horizontal lines in the wind direction plot are "wrap around" lines as the wind direction changes between slightly less and slightly greater than true North, and not an indication of large wind sweeps. The largest region of turbulence, above the expected high activity in the immediate vicinity of the ground, is between 1.5 and 2.0km, near the altitude of the top of Mt. Washington (1.9km). This could be the result of a Kelvin-Helmholtz instability due to the shear over the mountaintop. The high turbulence region is also right above a local maximum in humidity at about 70%, which is the start of an inversion in the temperature profile that persists through this ½ km band. It is not

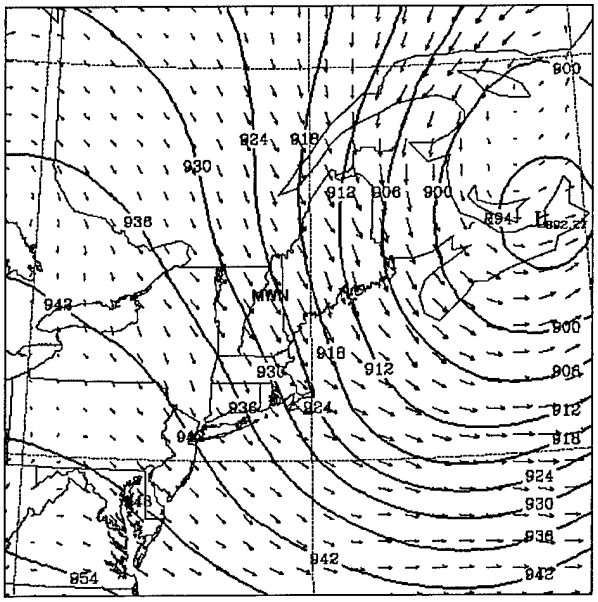

Figure 4. Weather analysis[16] showing a jet stream passing through northern New England at the time of the test. The 300hPa altitude contours show approximate jet streamlines, and the velocity vectors show relative speed and direction at summit height.

unusual to have increased turbulence at the top of a moisture layer. From 2km to 3km the C_n^2 level is somewhat reduced, followed by a region of increased C_n^2 between 3 and 3½ km. This higher region is located the start of a very dry layer. Then at 4km, the C_n^2 level drops by 3 orders of magnitude and enters the quiet region of the troposphere discussed above.

The quieter region is actually in the lower part of the jet stream, shown in Figure 4 depicting the winds over New England at that time. Referring to the wind speed part of Figure 2, the jet starts with a high shear region between 3km and above 4km, nearly coincident with the second region of high optical turbulence. The jet then increases to nearly 40m/s at around 10km, then it decreases to about 20m/s at 16km, and then decreases rapidly to about 5m/s. There is another region of higher turbulence around the upper jet shear region near 15km.

RESULTS

The C_n^2 data were then converted into estimates for ε following the equations presented above. The full profile of dissipation, and the intermediate steps of N^2 and *Ri* are shown in Figure 5. The large oscillations in N^2 are solely due to the small-scale changes in the vertical slope of the potential temperature, θ, which in turn is due to the changes in slope of the temperature, T. *Ri* is then obtained by dividing N^2 by the square of the vertical wind shear. The generally high Gradient Richardson Number indicates a generally stable atmosphere, and results in the γ function being held at unity for most of the flight. Only in the lower altitude regions below 3km, and spikes at around 7 and 10km does *Ri* drop below the 0.12 threshold to cause an increase in γ. The resulting profile in ε is shown in the third panel. It is highly variable over the profile. The highest dissipation is in the lower altitudes from the ground to twice the altitude of Mt. Washington.

An expanded view of the lowest 4km of the atmosphere is shown in Figure 6. There is a region of generally high turbulence in the lower altitudes with the highest peak, actually off the graph at 1.25, there is a minimum right above 1.4km. There is then a region of turbulence between 1.6 and 2km bounded by two peaks, followed by some activity, then a drop to a local minimum at 2.5km followed by a broad region of activity up to about 3.8km, with two spikes before dropping down immediately above 4km.

The next 5km segment is shown in Figure 7. This region is the lowest overall turbulence in the profile. Yet we see several thin regions of high dissipation. These are centered at: 5.2km, 5.7km, 6.4km, 7.2km, 7.7km8.75km, 9.3km, and 10km. While many of the peaks occur in nominally stable regions (Ri > 0.25), the strong, narrow spike at 7.2km occurs in the location of minimum Ri, and nearly zero potential temperature

gradient ($N^2 \sim 0$). This region at least suggests the presence of a nearly periodic mountain wave structure.

The next 5km segment, from 10km to 15km, is shown in Figure 8. This is the tropopause region, where the temperature gradient is increasing. This causes higher N^2 and generally higher values of Ri. In spite of the presumed higher stability, the number of regions of high dissipation increases, and appears more random than the lower 5km segment.

The upper 15km segment of the sounding is shown in Figure 9. The turbulence has settled into a stratospheric pattern. The increased stability, as demonstrated by the higher N^2 and Ri, results in thinner layers. There are a few regions of sustained high turbulence: the regions between 16 and 17km, between 23 and 24km, and thinner regions centered on 24.5, 26, 27, 28, and 29km.

COMPARISON TO LIDAR:

The dissipation rates estimated from the GroundWinds lidar[17] are compared to those from thermosonde launch NH_4 in Figure 10. The results are generally in fair agreement, with the notable exception of the largest spike in the thermosonde estimate at 1.2km. Referring back to the Figure 6, this spike occurred at a place where the Brunt-Väisälä frequency went to zero; the

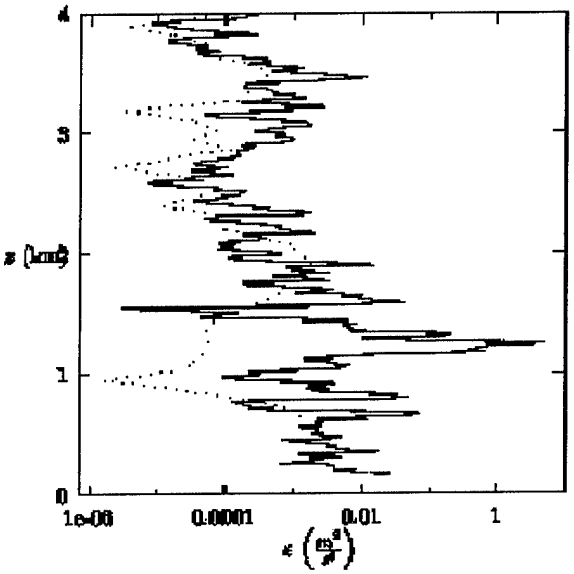

Figure 10. Comparison of dissipation rates as estimated from GroundWinds Lidar data (dotted) and from the Thermosonde data (solid).

Richardson number was near zero. Further, this spike is in the location of the high C_n^2 values associated with capping inversions mentioned earlier. This may have been in a small region of convectively unstable air that could have been outside the lidar beam.

If we ignore that region of disagreement, the results of the two methods are in fair agreement. There are two minimums in the lidar estimates on either side of 3km that are mirrored by the thermosonde estimates, although the lidar magnitudes are lower. The regions from about 1.6km to 2.5, and from 3.4 to 4.0 match very well.

CONCLUSIONS

Concurrent velocity sensing lidar and thermosonde measurements were made the evening of 31 May 2001 in the lee of Mt. Washington, New Hampshire. Data from each instrument was used to estimate the velocity turbulence dissipation rate. The thermosonde results were estimated using an extension of the radar power method described above. The results showed very high optical turbulence levels from ground level up to 4km, which is twice the altitude of Mt. Washington Summit. Above 4km there is a dramatic drop in optical turbulence followed by generally low levels until activity increases near the tropopause and in the higher shear regions of the jet stream.

At publication date, the available estimates of turbulence from the lidar are only the first 4km in altitude. The comparison of the two techniques is fair, with an obvious discrepancy near 1km, which may be due to an isolated convection cell, or other horizontally inhomogeneous feature.

ACKNOWLEDGEMENTS

The authors would like to thank Kris Robinson and George Clement, Stewart Radiance Laboratory, Utah State University, who are responsible for the successful thermosonde flights. We also gratefully acknowledge Ivan Dors, Space Science Center, University of New Hampshire for operating the lidar and analyzing the lidar data. We are also grateful to Dr. R. Beland, Air Force Research Laboratory, for financial and technical support of the thermosonde campaign.

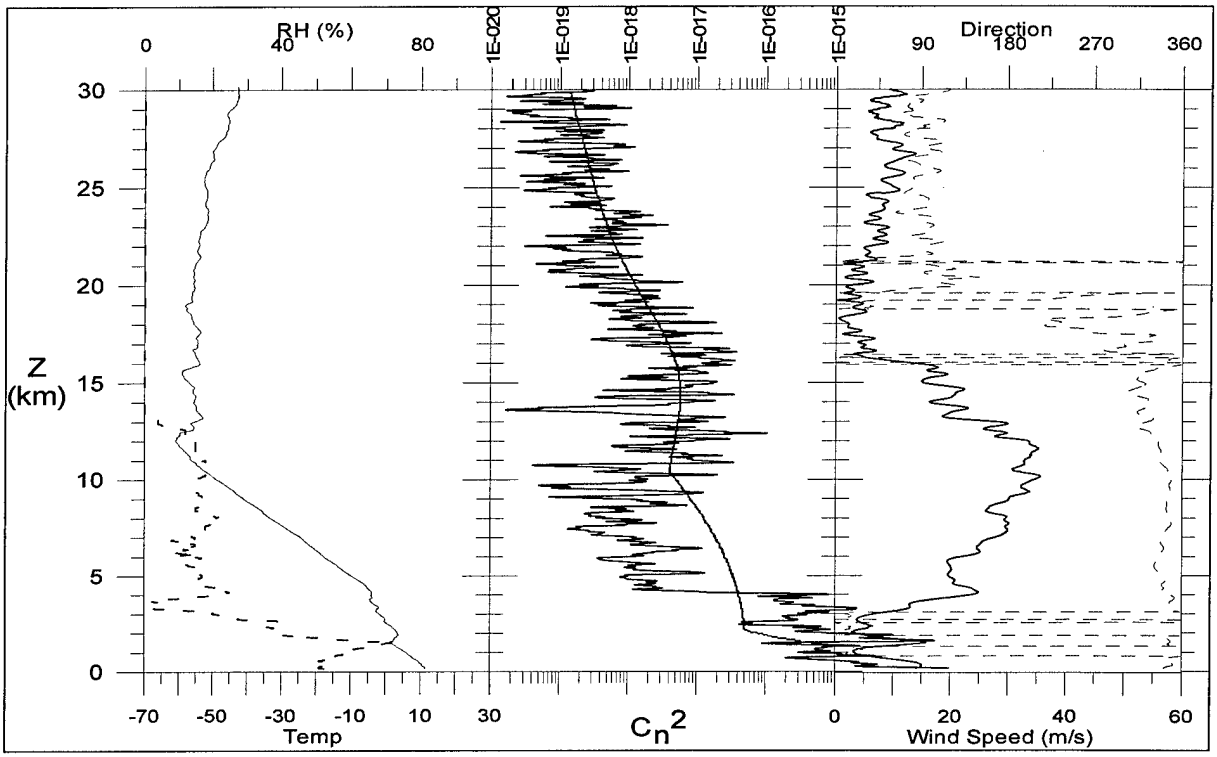

Figure 2. Profiles from thermosonde flight NH_4, Bartlett, NH on 31 May 2001. The left panel shows air temperature (solid) and relative humidity (dashed), the center shows C_n^2 along with the smoother Clear1 model profile, and the right panel shows wind speed (solid) and wind direction (dashed).

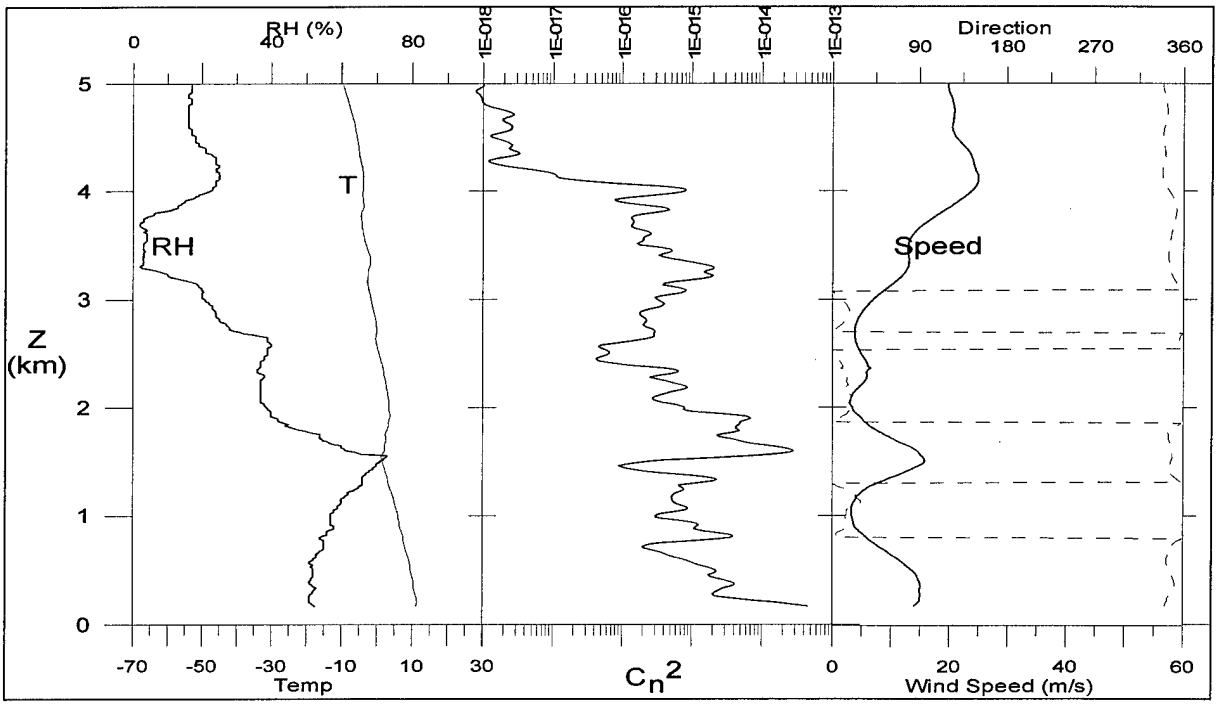

Figure 3. Profiles from the lowest 5km of thermosonde flight NH_4. See Figure 2 for variables.

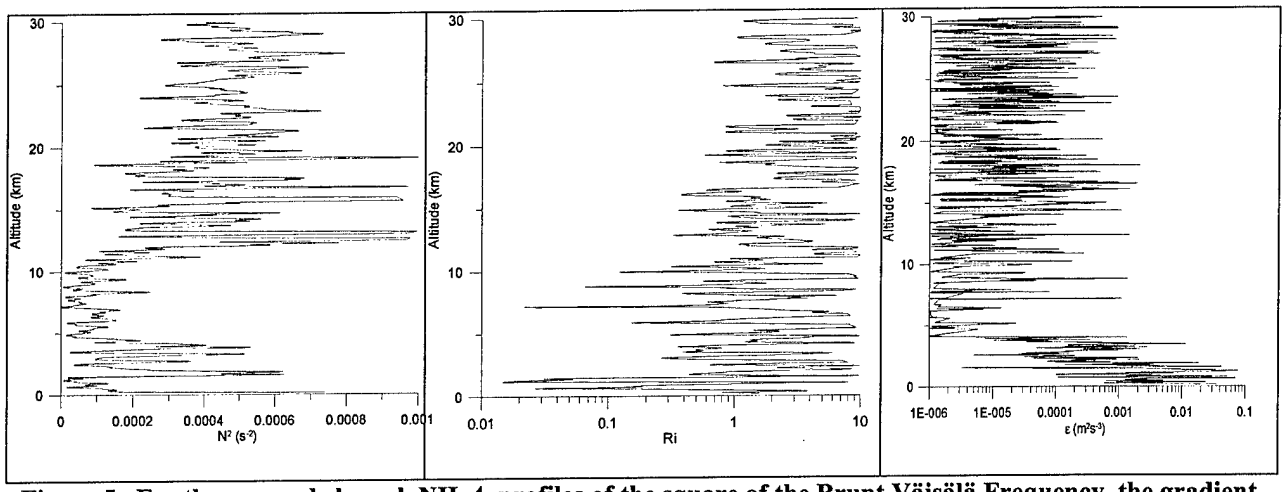

Figure 5. For thermosonde launch NH_4, profiles of the square of the Brunt Väisälä Frequency, the gradient Richardson Number, and the turbulent energy dissipation.

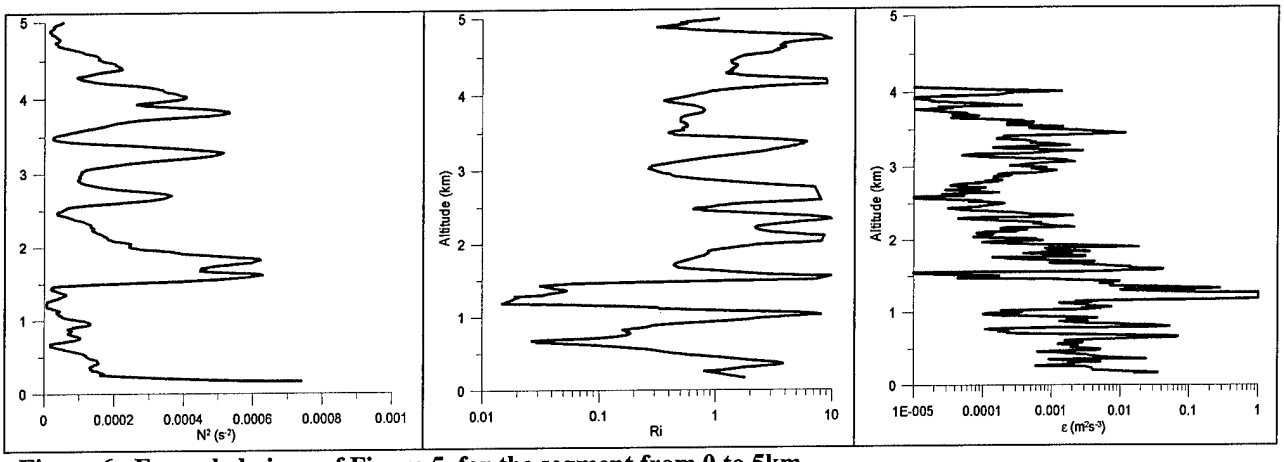

Figure 6. Expended views of Figure 5, for the segment from 0 to 5km.

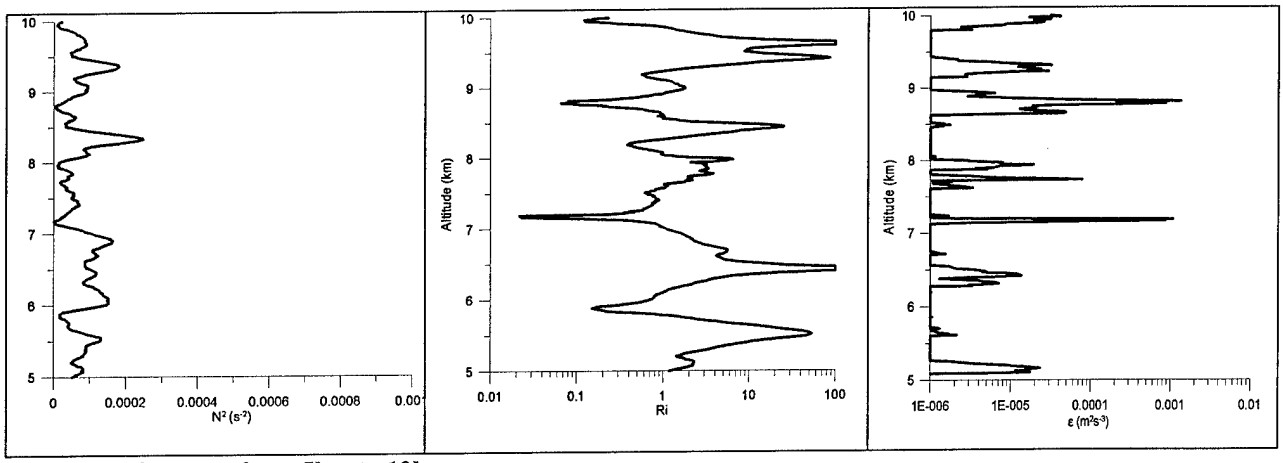

Figure 7. Segment from 5km to 10km.

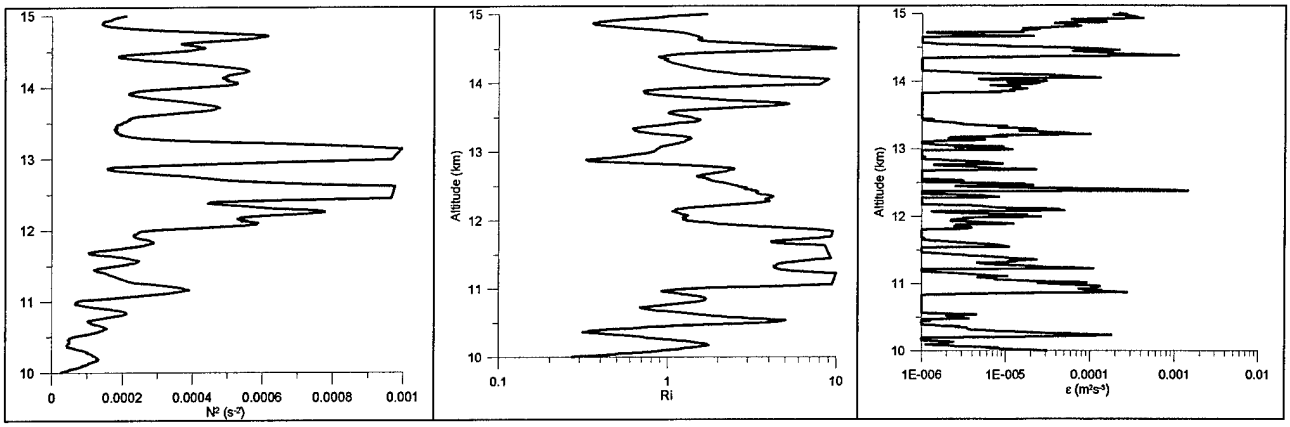

Figure 8. Segment from 10km to 15km.

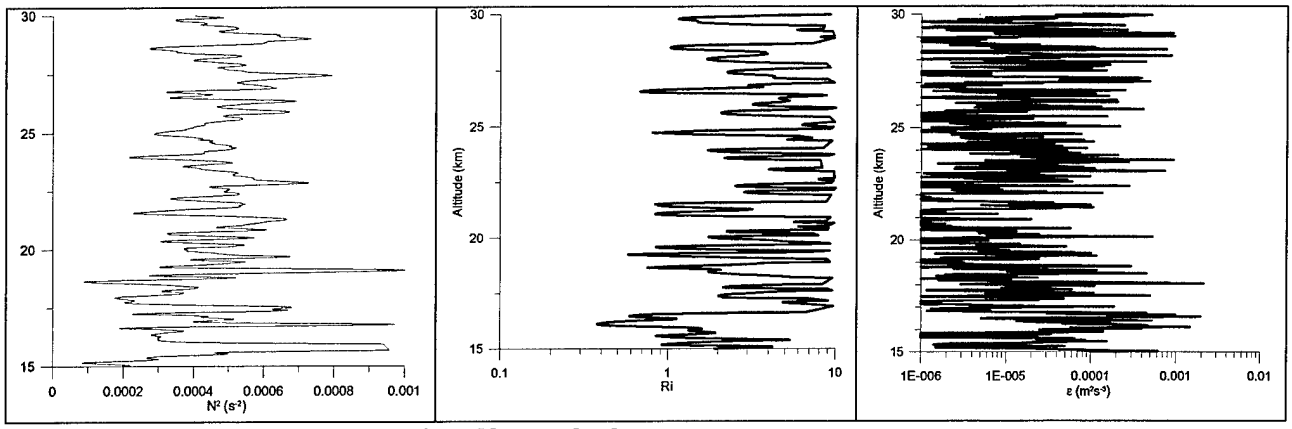

Figure 9. Upper 15km of the sounding. Note scale change

REFERENCES

[1] Kolmogorov, A.N., "The local structure of turbulence in incompressible viscous fluid for very large Reynolds numbers," Dokl. Akad. Nauk SSSR, Vol. 30, 4, 1941.

2 Paquin, J.E. and S. Pond, "The determination of the Kolmogoroff constants for velocity, temperature and humidity fluctuations from second- and third-order structure functions, J. Fluid Mech., vol. 50 (1971), part 2, pp. 257-269.

3 Ottersten, H., "Atmospheric structure and radar backscattering in clear air", Radio Science, Vol. 4, No. 12, 1969, pp. 1179-1193.

4 Hocking, W.K., "Measurement of turbulent energy dissipation rates in the middle atmosphere by radar techniques: A review", Radio Science, Vol. 23, No. 6, 1985, pp. 625-639.

5 Owens, J. C., "Optical refractive index of air: Dependence on pressure, temperature and compositions," Appl. Opt. 6, 1967, pp. 51-59.

6 Tatarski, V.I., Wave Propagation in a Turbulent Medium, McGraw-Hill, New York, 1961.

[7] VanZandt, T.E., J.L. Green, K.S. Gage, and W.L. Clark, "Vertical profiles of refractivity turbulence structure constant: Comparison of observations by the Sunset Radar with a new theoretical model", *Radio Science*, Vol. 13, No. 5, pp 819-829, 1978.

[8] Hocking, W.K. and P.K.L. Mu, "Upper and middle tropospheric kinetic energy dissipation rates from measurements of Cn2 – review of theories, in-situ investigations, and experimental studies using the Buckland Park atmospheric radar in Australia", Journal of Atmospheric and Solar-Terrestrial Physics, Vol. 59, No. 14, pp. 1779-1803, 1997.

9 Kundu, P.K., Fluid Mechanics, Academic Press, Inc., New York, 1990, p. 20.

10 Cohn, S.A., "Radar Measurements of Turbulent Eddy Dissipation Rate in the Troposphere: A Comparison of Techniques", J. Atmos. Oceanic Technol., 12, p. 85-95, 1995.

11 Bertin, F., J. Barat, and R. Wilson, "Energy dissipation rates, eddy diffusivity, and the Prandtl number: An in situ experimental approach and its consequences on radar estimates of turbulent parameters", Radio Science, Vol. 32, No. 2, pp. 791-804, 1997.

12 Jumper, G.Y., R.R. Beland, J.R. Roadcap, and O.R. Coté, "Effect of compressible flow on perceived temperature fluctuations measured by moving sensor", AIAA Journal, Vol. 37, No. 12, pp. 1609-1616, 1999.

13 Brown, J.H., R. E. Good, P.M. Bench, and G. Faucher, "Sonde measurements for comparative measurements of optical turbulence," Air Force Geophysics Laboratory, AFGL-TR-82-0079, ADA118740, NTIS, 1982.

14 Jumper, G.Y., H.M. Polchlopek, R.R. Beland, E.A. Murphy, P. Tracy, K. Robinson, "Balloon-borne measurements of atmospheric temperature fluctuations", AIAA-97-2353, 28th Plasmadynamics and Lasers Conference, June 23-25, 1997, Atlanta, GA.

15 Beland, R.R., "Propagation Through Atmospheric Optical Turbulence", The Infrared and Electro-Optical Systems Handbook, Vol. 2, Atmospheric Propagation of Radiation, edited by F.G. Smith, Infrared Information Analysis Center, Ann Arbor, MI, and SPIE Optical Engineering Press, Bellinghan, WA, 1993, pp. 157-232

[16] NOAA Air Resources Laboratory, from archived data accessed through the web site: http://www.arl.noaa.gov/ready/

[17] McHugh, J., "Inferring Velocity Turbulence Levels from Two Sensors", AIAA-2003-0190, 41st Aerospace Sciences Meeting, Reno, Nevada, Jan 2003.